Tropospheric and Ionospheric Effects in Spaceborne Single-Pass SAR Interferometry and Radargrammetry

Gerhard Krieger, DLR, Microwaves and Radar Institute, gerhard.krieger@dlr.de, Germany
Francesco De Zan, DLR, Microwaves and Radar Institute, francesco.dezan@dlr.de, Germany
Markus Bachmann, DLR, Microwaves and Radar Institute, markus.bachmann@dlr.de, Germany
Paco Lopez Dekker, DLR, Microwaves and Radar Institute, francisco.lopezdekker@dlr.de, Germany
Marc Rodriguez Cassola, Microwaves and Radar Institute, marc.rodriguez@dlr.de, Germany
Jun Su Kim, DLR, Microwaves and Radar Institute, junsu.kim@dlr.de, Germany

Abstract

It has often been claimed that spaceborne single-pass cross-track SAR interferometry is – up to an overall range shift – not affected by atmospheric effects. A closer analysis reveals, however, that both the troposphere and the ionosphere may cause notable phase, range and height offsets even in a single-pass interferometer. One such offset is due to slightly different incident angles which cause different path lengths through both the troposphere and the ionosphere. Another subtle effect arises from the wavenumber shift in combination with a dispersive medium like the ionosphere, which may induce differential range offsets in coherent radargrammetry. The analyses in this paper are not only of importance for future low-frequency bistatic SAR missions like Tandem-L, but they may also shed some new light on how the ionosphere can influence repeat-pass interferometry and radargrammetry in case of non-vanishing cross-track baselines.

1 Introduction

With the launch of TanDEM-X, spaceborne SAR interferometry has entered a new era. TanDEM-X is the first spaceborne single-pass SAR interferometer that enables the acquisition of cross-track and along-track interferograms with adjustable baseline lengths. Among the most remarkable features of the bistatic TanDEM-X satellite formation are the extraordinary precision of both the phase-synchronization link and the baseline determination which together allow for the generation of SAR interferograms with an 'absolute' phase accuracy of 10°-20° without referring to any ground control points [1], [2]. This phase corresponds to a range difference accuracy of 1-2 mm, as confirmed by evaluating repeated TanDEM-X data takes over a set of worldwide distributed test sites [3]. Assuming a height of ambiguity of 45 m, the absolute height accuracy for single data takes is therefore in the order of 2 m without use of any external height references. Thanks to this remarkable accuracy, several systematic second-order effects like gain-dependent delays or even relativistic effects have been revealed and used for improving both the calibration and interferometric processing of TanDEM-X data.

In this paper, we analyse how the atmosphere may affect the highly precise measurements provided by current and future spaceborne single-pass SAR interferometers. A large body of literature investigated wave propagation in the tropo- and ionosphere and their impact on SAR imaging and repeat-pass interferometry (cf. e.g. [4], [5], [6] and the references therein). In contrast, such analyses have not yet been performed in the context of single-pass SAR interferometry. This is, in part, due to the fact that it has often been claimed that single-pass interferometry is, up to a possible range and phase error common to both interferometric channels, not affected by the atmosphere. We will, however, show that both the troposphere and the ionosphere may cause vertical and horizontal DEM offsets of notable magnitude. The analyses in this paper are not only of fundamental interest for future single-pass SAR interferometers like Tandem-L, but they may also shed some new light on how the ionosphere could affect repeat-pass interferometry and radargrammetry in case of non-vanishing cross-track baselines.

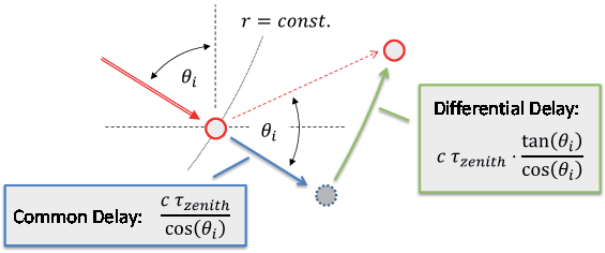

Figure 1: Change of interferometrically derived scatterer position due to common and differential atmospheric delay.

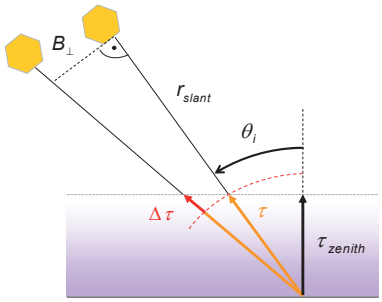

Figure 2: The slightly different incident angles cause a differential signal delay $\Delta\tau$ from the atmosphere. This delay may be mistaken as a differential range causing both a wrong topographic height and horizontal position estimate.

2 Tropospheric Effects

It is well known that the accurate geolocation of SAR images requires the precise consideration of tropospheric delays. These delays cause mainly a range shift along the line of sight as illustrated by the blue arrow in Figure 1. External knowledge of the tropospheric delay may therefore be used to reverse the additional range shift for each imaged scatterer [7]. Regarding single-pass SAR interferometry it has further been argued that the master and slave images receive the same delays, which seems to be justified due to the simultaneous data acquisition and the typically very small angular differences involved (for a TanDEM-X acquisition with a perpendicular cross-track baseline of 250 m, the distance between the rays at 10 km height is only 0.5 m). To check the implications of this assumption, we investigate a

ISBN 978-3-8007-3607-2 / ISSN 2197-4403

tropospheric model with a horizontally homogeneous layering (flat troposphere, cf. Figure 2). This model induces the additional (nondispersive) one-way range delay τ

$$\tau = \frac{\tau_{zenith}^{tropo}}{\cos\theta_i} \tag{1}$$

where τ_{zenith}^{tropo} is the one-way tropospheric zenith delay and θ_i the local incident angle. The differential delay for a small change in incident angle $\Delta\theta_i$ is then given by

$$\Delta\tau \approx \frac{\partial\tau}{\partial\theta_i}\cdot\Delta\theta_i = \tau_{zenith}^{tropo}\cdot\frac{\tan(\theta_i)}{\cos(\theta_i)}\cdot\Delta\theta_i \tag{2}$$

The angle $\Delta\theta_i$ can be approximated by $\Delta\theta_i \cong B_\perp/r_{slant}$ where $B_\perp$ is the baseline perpendicular to the line of sight and r_{slant} is the slant range distance from the satellite to the imaged area on the ground. If not corrected for, the differential delay $\Delta\tau$ is then mistaken as an additional range difference (or surplus interferometric phase) which yields, for a given scatterer on the ground, a wrong estimate of the angle of arrival at the single-pass interferometer. The error in the estimate of the angle of arrival $\Delta\beta$ is given by the ratio of the extra range $c\,\Delta\tau$ and the perpendicular baseline $B_\perp$. The wrong angle of arrival leads in turn to a shift Δs of the estimated scatterer position perpendicular to the line of sight (cf. green arrow in Figure 1). This shift is given by

$$\Delta s = \Delta\beta\cdot r_{slant} = \frac{c\,\Delta\tau}{B_\perp}\cdot r_{slant} = c\,\tau_{zenith}^{tropo}\cdot\frac{\tan(\theta_i)}{\cos(\theta_i)} \tag{3}$$

where we used the results from (2). The additional horizontal and vertical shifts Δx caused by the differential tropospheric delay are then given by

$$\begin{aligned}\Delta x_{horizontal}^{difftropo} &= \Delta s\cdot\cos(\theta_i) = c\,\tau_{zenith}^{tropo}\cdot\tan(\theta_i)\\ \Delta x_{vertical}^{difftropo} &= \Delta s\cdot\sin(\theta_i) = c\,\tau_{zenith}^{tropo}\cdot\tan^2(\theta_i)\end{aligned} \tag{4}$$

Taking into account also the common tropospheric delay, the overall horizontal and vertical shifts can be computed as

$$\begin{aligned}\Delta x_{horizontal}^{tropo} &= 2\,c\,\tau_{zenith}^{tropo}\cdot\tan(\theta_i)\\ \Delta x_{vertical}^{tropo} &= c\,\tau_{zenith}^{tropo}\cdot(\tan^2(\theta_i)-1)\end{aligned} \tag{5}$$

From (4) and (5) it becomes clear that the horizontal and vertical shifts depend only on the zenith delay and the incident angle, while the dependency on $B_\perp$ is canceled out.

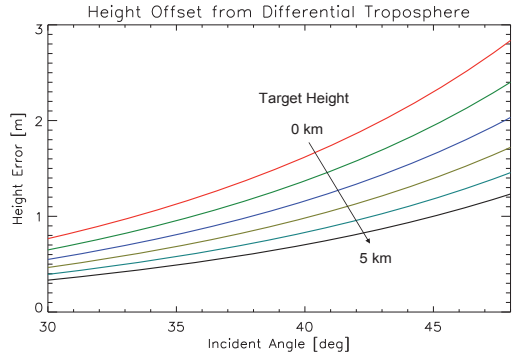

Figure 3: Predicted height offsets due to differential tropospheric delays. The height error increases for increasing incident angles. The decrease with increasing target height is caused by the lower amount of troposphere that is traversed by the radar echoes.

To quantify the expected magnitude of the height offsets caused by the differential tropospheric delay, we assume a very simple tropospheric model which is given by

$$c\cdot\tau_{zenith}^{tropo} = 2.3\text{ m}\cdot\exp\left(-\frac{h}{6000\,m}\right) \tag{6}$$

where h is the altitude of the considered scatterer above sea level. This simple model neglects, e.g., variations in sea level air pressure, temperature, or additional delays from varying water vapour and hydrometeors. All these contributions are typically smaller by one order of magnitude.

Figure 3 shows the height offsets from the differential troposphere as predicted by this model. The offsets are shown for different scatterer altitudes as a function of the incident angle. The minimum and maximum incident angles in this plot correspond to the near- and far-range beams used by TanDEM-X for global DEM acquisition. It becomes clear that the differential tropospheric delay will cause notable height offsets that systematically vary with the incident angle. Such offsets were indeed observed in the early phase of TanDEM-X DEM generation and are now absent after not only the common, but also the differential tropospheric delays have been taken into account in the interferometric processing chain (cf. Figure 4).

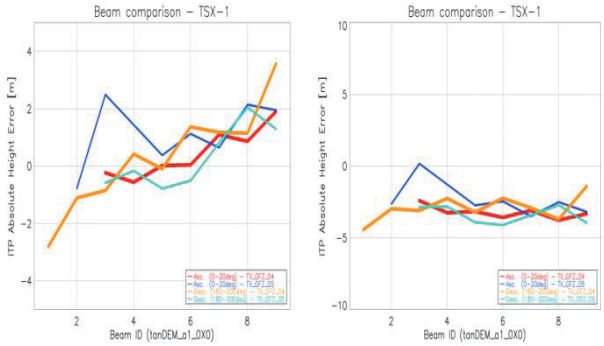

Figure 4: Observed height offsets in TanDEM-X as a function of the beam number (#1 and #9 correspond to incident angles of 30° and 48°, respectively). The different curves refer to ascending and descending orbits as well as to different baseline product revisions. Left: early processor version that included only the correction for the common tropospheric delay; Right: late processor version that included also the correction for the differential tropospheric delay.

3 Ionospheric Effects

3.1 Homogeneous Ionosphere

Similar to the tropospheric delays, the slightly different path lengths through a spatially homogeneous ionosphere may cause an absolute and differential ionospheric delay. Due to the dispersive character of the ionosphere one should, however, differentiate between group delay and phase advance. Modelling the ionosphere as a plasma where only the electrons are moving in response to the waves' electric field, the one-way zenith delay can be approximated to first order as

$$\tau_{zenith}^{iono,group} = -\tau_{zenith}^{iono,phase} = \frac{K}{cf^2}TEC \tag{7}$$

where f denotes frequency, TEC is the total number of electrons per unit area in a vertical column from the Earth surface up to the satellite height and $K = 40.28\ \text{m}^3/\text{s}^2$

ISBN 978-3-8007-3607-2 / ISSN 2197-4403

can be easily derived from the electron mass, elementary charge and free space permittivity. This approximation neglects all contributions that will arise from a magnetic field in the direction of propagation (cf. Lassen-Appleton-Hartree equation), but it is nevertheless sufficiently accurate for a first-order evaluation as intended in this paper. The total electron density TEC is often expressed in TEC units (TECUs) where one TECU corresponds to 10^{16} electrons per meter squared. Depending on geographic location, solar activity, season and local time of day, typical TEC values may range from <1 TECU to more than 100 TECUs.

To get a first idea about the magnitude of the expected vertical and horizontal DEM offsets introduced by the ionosphere, we model the ionosphere again as a spatially homogeneous medium. In a first step, we may also neglect the curvature of the ionosphere. Assuming now, for example, in (7) a total electron content of 40 TECU in a vertical column below the radar satellites, the predicted height offsets from the common ionospheric component are -10.3 m and -17 cm for L- and X-band, respectively. To account for the differential component, one has to distinguish between phase advance and group delay which cause opposite offsets for radargrammetrically and interferometrically derived DEMs as illustrated in Figure 5.

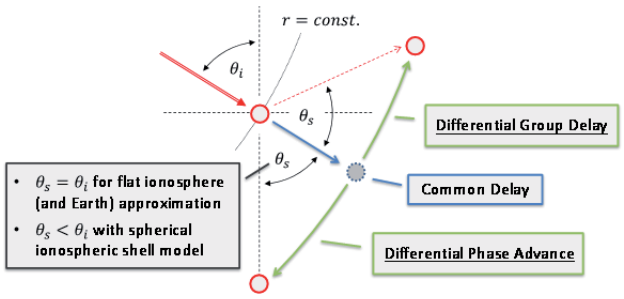

Figure 5: The different signs for ionospheric phase advance and group delay cause a mutual offset between interferometrically and radargrammetrically derived DEMs.

For the flat ionosphere approximation we may again use (4) to derive the vertical and horizontal errors, but we should now employ negative signs in case of interferometry. A simple case arises for an incident angle of 45°, where the contributions from the absolute and differential ionosphere become equal (only true for flat ionosphere approximation, cf. Figure 5). As a result, the interferometric DEM will experience for the previously assumed total electron content of 40 TECU vertical shifts of -20.6 m and -34 cm for L- and X-band, respectively, while there is no vertical shift in the radargrammetric DEM under this specific assumption. It is evident that ionospheric height offsets of this order of magnitude will be clearly visible in L-band DEMs while they will only marginally be detectable in small baseline X-band DEMs. Figure 6 shows the predicted horizontal and vertical offsets based on a more refined evaluation that models the ionosphere not as a flat layer but as a narrow spherical shell of various heights (for reference, the dashed curves correspond to a spherical shell height of 0 m which is equivalent to the previous flat ionosphere approximation). Taking into account the additional spectral shift contribution to be described in Section 3.2, the systematic offsets between radargrammetric and interferometric DEMs may be exploited for absolute TEC estimates and the derivation of appropriate height corrections in a single-pass SAR interferometer.

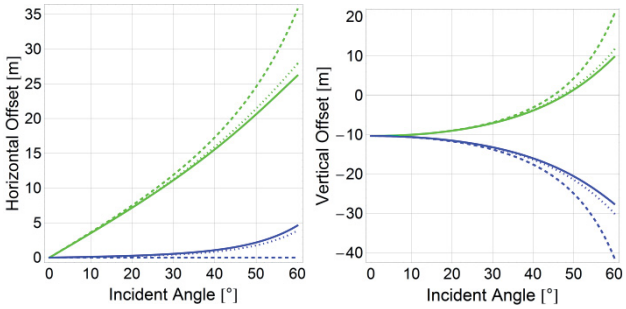

Figure 6: Predicted horizontal (left) and vertical (right) ionospheric shifts for an L-band single-pass SAR interferometer operating at a vertical TEC of 40 TECU. The different colours refer to radargrammetric (green) and interferometric (blue) DEM generation. A spherical ionospheric shell model is assumed with shell heights of 400 km (solid), 300 km (dotted) and 0 km (dashed). Note that the additional spectral shift component has not yet been incorporated in these plots.

3.2 Impact of Spectral Shift

Another subtle effect arises from the dispersive nature of the ionosphere in combination with non-vanishing interferometric cross-track baselines. To understand this effect, we should distinguish between a scenario with widely separated point scatterers and a distributed scatterer scenario. For the latter, both the radargrammetric and the interferometric combination of two SAR images acquired from slightly different incident angles implies the coherent combination of different range frequency components to match their wavenumbers parallel to the imaged surface [8]. As a result, the radargrammetric and interferometric measurements are implicitly formed from two SAR images that have different centre frequencies and which experience therefore different phase and group delays. Assuming ideal correlation of the complex image pair, the co-registration offset induced by the dispersive ionosphere can be expressed as [9]

$$\Delta\tau_{specshift}^{iono,group} = -\frac{2K}{cf_0^3}\cdot\left(\Delta f + \frac{1}{2f_0}\Delta f^2 + \cdots\right)\cdot STEC \quad (8)$$

where STEC denotes slant TEC (i.e. total electron content along the line of sight). Assuming a spectral shift of 20 MHz and a vertical TEC of 40 TECU we obtain for an incident angle of 45° differential two-way range shifts of approx. -47 cm and -1 mm in L- and X-band, respectively. For a bistatic single-pass SAR interferometer the range frequency shift to obtain the same wavenumbers on the ground is given by [8]

$$\Delta f = -\frac{f_0 B_\perp}{2\, r_{slant}\tan(\theta_i-\alpha)} = -\frac{f_0}{2\tan(\theta_i-\alpha)}\cdot\Delta\theta_i \quad (9)$$

where α denotes a possible local slope angle. By substituting the spectral shift Δf from (9) into (8), we obtain in analogy to (3) and (4) the vertical and horizontal shifts of the radargrammetric DEM

$$\begin{aligned} dx_{horizontal}^{iono,specshift} &\cong \frac{K}{f_0^2}\cdot\frac{\cos(\theta_i)}{\tan(\theta_i-\alpha)}\cdot STEC \\ dx_{vertical}^{iono,specshift} &\cong \frac{K}{f_0^2}\cdot\frac{\sin(\theta_i)}{\tan(\theta_i-\alpha)}\cdot STEC \end{aligned} \quad (10)$$

Figure 7 shows the additional radargrammetric DEM offsets that will arise from the ionospheric spectral shift dispersion for a distributed scatterer scenario.

ISBN 978-3-8007-3607-2 / ISSN 2197-4403

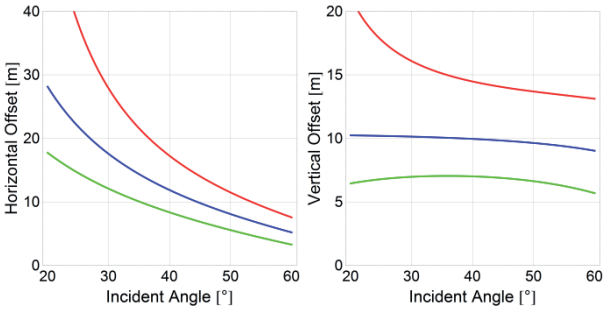

Figure 7: Predicted additional horizontal (left) and vertical (right) radargrammetric DEM offsets for a distributed scatterer scenario in L-band assuming a vertical TEC of 40 TECU. The different colours refer to local slopes of 10° (green), 0° (blue), and -10° (red). The modelled height of the ionospheric shell is 350 km. Note that this radargrammetric DEM offset arises in addition to the offsets from Figure 6.

We may now ask the question whether the interferometric DEM acquisition is also affected by the ionospheric spectral shift dispersion. For this, we assume again perfect co-registration by means of complex cross-correlation[1]. In [9] we show that the interferometric phase offset can in this case be well approximated by

$$\Delta\varphi_{interfero}^{iono,specshift} \cong \frac{4\pi K}{cf_0^2}\left(\Delta f + \frac{\Delta f^2}{2f_0}\right) STEC \qquad (11)$$

In interpreting the phase offset from this formula, we have, however, to take care that we do not count phase offsets twice. The linear Δf term in (11) is related to the common shift of the two interferometric channels and has already been taken into account when we computed the vertical and horizontal offsets in Section 3.1. The residual contribution is therefore provided by the quadratic term in (11). Assuming again a spectral shift of 20 MHz and a vertical TEC of 40 TECU we obtain, for an incident angle of 45°, phase errors of 5.6° and 0.01° in L- and X-band, respectively.

3.3 Ionospheric Gradients and Turbulence

The previous analyses were based on a ionospheric model with spatially constant (i.e. homogeneous) TEC values. Real ionospheric conditions are, however, often characterized by inhomogeneous TEC concentrations. The impact of linear TEC gradients and stochastic TEC perturbations on single-pass SAR interferometry have, together with several further effects, been analysed in [9]. Figure 8 shows, as an example, the predicted additional interferometric phase errors for a turbulent ionosphere, where the variations in local electron density are described by a stochastic power-law model. The interferometric phase errors are shown as a function of the incident angle difference $\Delta\theta_i$, where $\Delta\theta_i = 0.2°$ translates in L-band, for $\theta_i = 45°$, to a height of ambiguity of 48 m. A phase error of 30° would therefore cause a local height offset of 4 m.

[1] As pointed out by one reviewer, it makes a difference whether co-registration is performed purely on geometric information or by cross-correlation. The former will lead to a phase error in accordance with (8) and (9). It makes, moreover, a difference whether co-registration is coherent or incoherent, and whether point or distributed targets dominate. We thank the reviewer for these valuable comments and will provide a discussion in [9]. In this light, our phase offset estimate in (11) may be regarded as a lower bound that can be achieved by optimum data-driven co-registration.

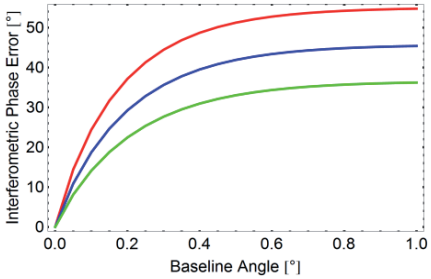

Figure 8: Interferometric phase errors of an L-band single-pass SAR interferometer for a turbulent ionosphere. The figure shows the standard deviation of the expected errors as a function of the incident angle difference $\Delta\theta_i$. In this example, the total electron content of the background ionosphere is 40 TECU and the percentage of its variable content is 2% (corresponding to a vertically integrated strength of turbulence $C_k L = 6.5 \cdot 10^{33}$). The spectral index and outer scale length are 3.5 and 10 km, respectively. The incident angle is $\theta_i = 45°$ and the different curves refer to azimuth resolutions of 6 m (green), 12 m (blue), and 12 km (red).

4 Conclusions

This paper provided first steps towards a systematic assessment of how atmospheric wave propagation affects interferometry and radargrammetry in a spaceborne bistatic single-pass SAR interferometer. Absolute and differential delays in the homogeneous troposphere and ionosphere cause significant vertical and horizontal DEM offsets. Coherent radargrammetry is additionally affected by spectral shift in combination with dispersive wave propagation in the ionosphere. Additional errors arise from ionospheric turbulence, which causes phase and height fluctuations at typical scales in the order of 1-10 km. Detailed derivations and a discussion of further effects will be provided in [9].

References

[1] G. Krieger, M. Zink, M. Bachmann et al., "TanDEM-X: A Radar Interferometer with Two Formation-Flying Satellites", Acta Astronautica, Vol. 89, pp. 83-98, 2013.

[2] C. Rossi, F. Rodriguez Gonzalez, T. Fritz, N. Yague-Martinez, M. Eineder, "TanDEM-X Calibrated Raw DEM Generation", ISPRS Journal of Photogrammetry and Remote Sensing, Vol. 73, pp. 12-20, 2012.

[3] J.W. Antony, J. Hueso Gonzalez, M. Bachman, M. Schwerdt, G. Krieger, M. Zink, "Results of the TanDEM-X Baseline Calibration", IEEE J. Select. Topics Earth Obs. Remote Sens., Vol. 6, No. 3, pp. 1495-1501, 2013.

[4] R. Hansen, "Radar Interferometry", Kluwer Academic Publishers, Dordrecht, 2001.

[5] Z.W. Xu, J. Wu, Z.-S. Wu, "A Survey of Ionospheric Effects on Space-Based Radar", Waves in Random Media, Vol. 14, pp.189-273, 2004.

[6] F. Meyer, R. Bamler, N. Jakowski, T. Fritz, "The Potential of Low-Frequency SAR Systems for Mapping Ionospheric TEC Distributions", IEEE Geosci. Remote Sens. Letters, Vol. 3, pp. 560-564, 2006.

[7] M. Eineder, C. Minet, P. Steigenberger, X. Cong, T. Fritz, "Imaging Geodesy - Toward Centimeter-Level Ranging Accuracy with TerraSAR-X", IEEE Trans. Geosci. Remote Sens., Vol. 49, pp. 661-671, 2011.

[8] F. Gatelli, A. Monti Guarnieri, F. Parizzi, P. Pasquali, C. Prati, F. Rocca, "The Wavenumber Shift in SAR Interferometry", IEEE Trans. Geosci. Remote Sens., Vol. 32, pp. 855-865, 1994.

[9] G. Krieger, F. De Zan, et al., Manuscript to be submitted to IEEE Transactions on Geoscience and Remote Sensing, 2014.

ISBN 978-3-8007-3607-2 / ISSN 2197-4403